Unal, G.B. & Slabaugh, G.G. (2005). Coupled PDEs for Non-Rigid Registration and Segmentation. In: 2005 IEEE Computer Society Conference on Computer Vision and Pattern Recognition Workshops. (pp. 168-175). IEEE Computer Society. ISBN 0-7695-2372-2

CITY UNIVERSITY LONDON

Coupled PDEs for Non-Rigid Registration and Segmentation

Gozde Unal Greg Slabaugh
Intelligent Vision and Reasoning Department
Siemens Corporate Research
Princeton, NJ 08540

Abstract

In this paper we present coupled partial differential equations (PDEs) for the problem of joint segmentation and registration. The registration component of the method estimates a deformation field between boundaries of two structures. The desired coupling comes from two PDEs that estimate a common surface through segmentation and its non-rigid registration with a target image. The solutions of these two PDEs both decrease the total energy of the surface, and therefore aid each other in finding a locally optimal solution. Our technique differs from recently popular joint segmentation and registration algorithms, all of which assume a rigid transformation among shapes. We present both the theory and results that demonstrate the effectiveness of the approach.

1. Introduction

Detection of specific anatomic structures in medical images or volumes is an important research problem in Computer Aided Diagnosis (CAD) applications. By a detection method we refer to a segmentation for outlining a target structure plus a registration in the presence of multiple images of the same structure or region. In many medical imaging applications multiple number of image volumes in which a structure of interest resides are available. Different modality images of the same region may also be available in some applications. The challenge is then to make use of and relate the existing extra information from several given image volumes. Many methods dealing with the detection problem in multiple images have been proposed. In one class of methods, first the target region is segmented separately in both images, then the resulting boundaries or regions are registered. In another class of methods, a global or local registration of the two images is carried out first, then the target region is segmented using information coming from both images. In this paper, we address estimation of boundaries of a target structure in two image volumes in the presence of nonrigid deformations that are also estimated simultaneously.

1.1. Relation to previous work

There is a vast literature on segmentation of anatomical structures. Particularly, deformable models have been popularly used in medical image segmentation problems, see [12] for a survey. Similarly for registration of medical structures, a tremendous amount of work has been done, see surveys [4, 11], or for mutual information-based techniques see [17]. Recently, there has been an interest in combining segmentation and registration problems due to a strong interdependence between these two challenging problems of medical image analysis. Many of the methods developed in this context used shape prior models in an energy minimization framework [7]. For instance, in [16], a shape model based on a level set representation is constructed and used in an energy to force the evolving interface to align rigidly with the prior shape. The segmentation energy is separately involved as a boundary and region based energy model. In [19], similarly, a boundary based energy or a Mumford-Shah energy is utilized in conjunction with a distance to a shape prior to which the evolving contour is transformed by a rigid motion. In the same work, the authors also presented an intensity-based PDE which evolves a source image towards a target image, and a coupling PDE to solve for the coordinate transformation from source to the target. This approach however involves a pre-segmentation step, hence is not a joint segmentation and registration approach. Using different criteria for segmentation and rigid registration in an iterative/sequential manner has been carried out in a Bayesian framework [20]. The same idea of simultaneous segmentation and rigid registration with a prior shape model has been applied to time-varying data for motion estimation and segmentation of moving structures, particularly in cardiac imaging [9]. An active region model based on classical snake nodal constraints with a displacement field defined over the nodes is utilized for again a combined segmentation and motion tracking goal in heart imaging.

Almost all of the methods listed above involve only rigid registration as the transformation between two shapes or images. However, for shapes which non-rigidly show up in different images, all of these approaches will fail. For instance, a synthetic binary image volume shown in green in Figure 1 has deformed into the binary image volume shown in red and our goal is to segment the 3D shape from the given multiple image volumes and simultaneously capture the deformation among these volumes.

Figure 1. Two binary image volumes which have a non-rigid correspondence (visualized by their zero level sets).

Nonetheless, this work is also distantly related to a multitude of tracking techniques, such as [1, 3] that used a region matching through an optical flow constraint, [15, 8] that used a parametric motion model, [23] that matched the distribution of a region with a prior model distribution, or region matching through segmented contours as boundary constraints for registration [18].

On the other hand, it is worth mentioning approaches developed solely for the purpose of nonrigid registration, a popular class of which are variational as well, solve PDEs for the purpose of non-rigid matching between two image volumes [2, 1, 6]. These techniques are aimed at globally registering image volumes and therefore estimate the deformation field over the whole image. Our technique also solves for a deformation field, however the field is only over the surface. In addition, we also solve for the segmentation in multiple images jointly with the registration.

1.2. Our contribution

The contribution of this paper is to develop a joint non-rigid registration and segmentation method without relying on shape priors. If required by the application though, the shape priors can easily be incorporated into the framework we build. We generalize the joint segmentation and registration work of Yezzi et al. [21, 22] which estimates rigid registration parameters between two images and a segmentation in a coupled way. An overall energy functional depending on two image regions and registration parameters is minimized resulting in PDEs of both the contour and the registrations through a level set representation [14]. In [22], finite dimensional registrations are involved, but an extension to infinite dimensions is not foreseen. For instance, application of this rigid registration method to the binary image volumes in Fig. 1 will result in a best rigid fit of the first volume onto the second one as shown in Figure 2. In

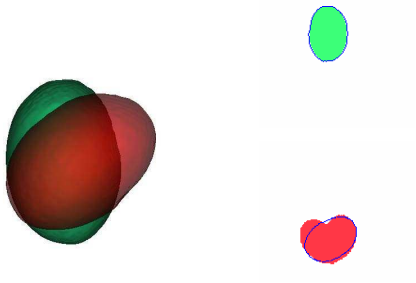

Figure 2. Rigid registration on binary image volumes that do not have a rigid correspondence fails. On the right shown are a slice from both image volumes with the converged surface (2D blue contour at the slice).

this paper, we start with the same joint segmentation and registration idea however improve it to account for more general problems of registration among anatomical structures defined by a deformation field or a displacement field between target regions. The applications are vast such as structures in different MR image sequences (for instance T1 and T2 weighted) or pre and post contrast agent MR images or images of a patient at different time points or images of different patients as well as images of different modalities. Our method performing on the same binary image volume pair is seen in Figure 3 where the green volume is correctly deformed towards the red volume.

The organization of the paper is as follows. We first briefly present background information on finite-dimensional joint registration and segmentation in Section 2. We then present a novel technique for an infinite-dimensional registration jointly with segmentation in Section 3. Results and conclusions are given in Section 4 and 5 respectively.

2. Background: Joint rigid registration and segmentation

Given two images $I : \Omega \longrightarrow \mathbb{R}^2$ and $\hat{I} : \Omega \longrightarrow \mathbb{R}^2$, the transformation that deforms one of the images to the other one is denoted by: $g : \mathbb{R}^2 \longrightarrow \mathbb{R}^2$, which is an element of a finite dimensional group G with parameters $g_1, ..., g_n$. The goal is to find a curve $\boldsymbol{C} \in \Omega$ that deforms on the first image I whereas a curve $\hat{\boldsymbol{C}} \in \hat{\Omega}$ corresponding to the mapping $\hat{\boldsymbol{C}} = g(\boldsymbol{C})$ deforms on the second image $\hat{I}$. Both contours move according to a generic region-based energy

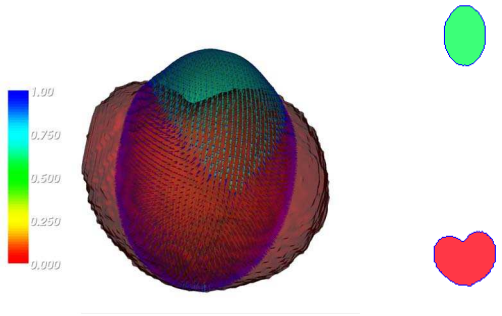

Figure 3. Non-rigid registration on the same binary image volumes successfully deform the surface on the green image volume into a surface on the red image volume. On the right shown are a slice from both image volumes with the final surface (2D blue contour at the slice). Also shown on the green surface is the vector field pointing correctly towards the red surface.

functional defined over both image domains as follows:

$$E(\boldsymbol{C}, g) = \int_{\boldsymbol{C_{in}}} f_{in}(\boldsymbol{x})d\boldsymbol{x} + \int_{\boldsymbol{C_{out}}} f_{out}(\boldsymbol{x})d\boldsymbol{x} + \int_{\hat{\boldsymbol{C}}_{\boldsymbol{in}}} \hat{f}_{in}(\hat{\boldsymbol{x}})d\hat{\boldsymbol{x}} + \int_{\hat{\boldsymbol{C}}_{\boldsymbol{out}}} \hat{f}_{out}(\hat{\boldsymbol{x}})d\hat{\boldsymbol{x}} + \int_{\boldsymbol{C}} ds \quad (1)$$

where f_{in} and f_{out} are the region descriptors inside and outside contour $\boldsymbol{C}$ respectively (same comments apply for $\hat{f}_{in}$ and $\hat{f}_{out}$ for $\hat{\boldsymbol{C}}$), and the last term represents the regularization on the unknown curve $\boldsymbol{C}$. This energy is re-expressed in terms of integrals only over the space Ω as follows:

$$E(\boldsymbol{C}, g) = \int_{\boldsymbol{C_{in}}} (f + |g'|\hat{f}\cdot g)(\boldsymbol{x})d\boldsymbol{x} + \int_{\boldsymbol{C_{out}}} (f + |g'|\hat{f}\cdot g)(\boldsymbol{x})d\boldsymbol{x} + \int_{\boldsymbol{C}} ds \quad (2)$$

where $f = f_{in} - f_{out}$, $\hat{f} = \hat{f}_{in} - \hat{f}_{out}$, g' denotes the Jacobian of g, and $\cdot$ denotes functional composition. The gradient descent flow for evolution of the curve $\boldsymbol{C}$ can be obtained as $\boldsymbol{C}_t = [(f + |g'|\hat{f}\cdot g) + \kappa]\boldsymbol{N}$, where κ is the curvature, and $\boldsymbol{N}$ is the normal of the curve. The case of rigid registration, which is a special case among finite-dimensional registration groups, amounts to representing g by a rotation matrix $\boldsymbol{R}$ and a translation vector $\boldsymbol{t}$ as: $g(\boldsymbol{x}) = \boldsymbol{R}\,\boldsymbol{x} + \boldsymbol{t}$. The gradient evolutions for the registration parameters g_i then are given by [22]

$$\frac{\partial g_i}{\partial t} = \int_C \hat{f}(g(\boldsymbol{x})) < \frac{\partial g(\boldsymbol{x})}{\partial g_i}, \boldsymbol{R}\boldsymbol{N} > ds. \quad (3)$$

In the next section we present a generalization of this technique from a finite dimensional transform $\hat{\boldsymbol{x}} = g(\boldsymbol{x})$ to an infinite-dimensional transform $\hat{\boldsymbol{x}} = T(\boldsymbol{x})$ where each point in domain Ω can move freely to a point in domain $\hat{\Omega}$ as depicted in Figure 4.

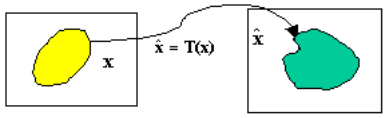

Figure 4. Non-rigid mapping between two images defined through the coordinate transformation: $T(\boldsymbol{x}) = \boldsymbol{x} + \boldsymbol{u}$.

3. A joint non-rigid registration and segmentation approach

Given two image volumes, we denote the transformation that deforms one of the images to the other one by: $\hat{\boldsymbol{x}} = \boldsymbol{T}(\boldsymbol{x}) = \boldsymbol{x} + \boldsymbol{u}(\boldsymbol{x})$, where $\boldsymbol{u}(\boldsymbol{x})$ is the displacement vector field defined as $\boldsymbol{u} : \Omega \longrightarrow \mathbb{R}^n$ ($n = 2$ or 3).

The general region-based energy functional for joint segmentation and registration can be re-written as follows:

$$E(\boldsymbol{S}, \boldsymbol{u}) = \int_{\boldsymbol{S_{in}}} f_{in}(\boldsymbol{x})d\boldsymbol{x} + \int_{\boldsymbol{S_{out}}} f_{out}(\boldsymbol{x})d\boldsymbol{x} + \int_{\boldsymbol{S}} dA + \int_{\hat{\boldsymbol{S}}_{\boldsymbol{in}}} \hat{f}_{in}(\hat{\boldsymbol{x}})d\hat{\boldsymbol{x}} + \int_{\hat{\boldsymbol{S}}_{\boldsymbol{out}}} \hat{f}_{out}(\hat{\boldsymbol{x}})d\hat{\boldsymbol{x}} + \frac{\beta}{2}\int_{\Omega} ||\nabla \boldsymbol{u}||^2 d\boldsymbol{x} \quad (4)$$

where the last two terms on each line represent the regularization on the unknown surface $\boldsymbol{S}$ and vector field $\boldsymbol{u}$, $\hat{\boldsymbol{x}} = \boldsymbol{x} + \boldsymbol{u}(\boldsymbol{x})$, and f_{in}, f_{out}, and $\hat{f}_{in}$, $\hat{f}_{out}$ are as before for the first image and the second image respectively. β is a fixed parameter, e.g. 0.5, to weight the amount of smoothing on the vector field $\boldsymbol{u}$.

The solutions to the minimization problems are given by:

$$\tilde{\boldsymbol{S}} = \arg\min_{\boldsymbol{S}} E(\boldsymbol{S}, \boldsymbol{u}), \quad \text{and} \quad \tilde{\boldsymbol{u}} = \arg\min_{\boldsymbol{u}} E(\boldsymbol{S}, \boldsymbol{u}) \quad (5)$$

Let us reformulate the problem in terms of a level set function $\Phi : \Omega \longrightarrow \mathbb{R}$ which represents $\boldsymbol{S}$ as its zero level set. Let H denote a Heaviside function, then E in (4) can be re-written as:

$$E(\Phi, \boldsymbol{u}) = \int_{\Omega} f_{in}(x)H(\Phi(\boldsymbol{x}))d\boldsymbol{x} + \int_{\Omega} f_{out}(\boldsymbol{x})(1 - H(\Phi(\boldsymbol{x})))d\boldsymbol{x} + \int_{\hat{\Omega}} \hat{f}_{in}(\hat{\boldsymbol{x}})H(\hat{\Phi}(\hat{\boldsymbol{x}}))d\hat{\boldsymbol{x}} + \int_{\hat{\Omega}} \hat{f}_{out}(\hat{\boldsymbol{x}})(1 - H(\hat{\Phi}(\hat{\boldsymbol{x}})))d\hat{\boldsymbol{x}} + \int_{\Omega} \delta(\Phi)|\nabla\Phi|d\boldsymbol{x} + \frac{\beta}{2}\int_{\Omega} ||\nabla \boldsymbol{u}(\boldsymbol{x})||^2 d\boldsymbol{x} \quad (6)$$

where $\hat{\Phi}(\boldsymbol{x} + \boldsymbol{u}) = \Phi(\boldsymbol{x})$ and $\delta(\boldsymbol{x}) = dH(\boldsymbol{x})/d\boldsymbol{x}$ in the sense of distributions. Indeed, we used regularized versions

of $H(\boldsymbol{x})$ and $\delta(\boldsymbol{x})$ given in [5]. The surface evolution in this case is given by:

$$\frac{\partial \Phi}{\partial t} = \delta(\Phi) f(\boldsymbol{x}) + \delta(\hat{\Phi}(\boldsymbol{x} + \boldsymbol{u}(\boldsymbol{x}))) \hat{f}(\boldsymbol{x} + \boldsymbol{u}(\boldsymbol{x})) + \kappa. \tag{7}$$

For registration evolution, the only part of the energy functional in Eq. (6) that is taken into account is:

$$\begin{aligned} E(\boldsymbol{u}) &= \int_\Omega \underbrace{\hat{f}_{in}(\boldsymbol{x} + \boldsymbol{u}(\boldsymbol{x})) H(\hat{\Phi}(\boldsymbol{x} + \boldsymbol{u}(\boldsymbol{x})))}_{F_{in}(\boldsymbol{x} + \boldsymbol{u}(\boldsymbol{x}))} d\boldsymbol{x} \\ &\quad + \int_\Omega \underbrace{\hat{f}_{out}(\boldsymbol{x} + \boldsymbol{u}(\boldsymbol{x}))(1 - H(\hat{\Phi}(\boldsymbol{x} + \boldsymbol{u}(\boldsymbol{x}))))}_{F_{out}(\boldsymbol{x} + \boldsymbol{u}(\boldsymbol{x}))} d\boldsymbol{x} \\ &\quad + \frac{\beta}{2} \int_\Omega ||\nabla \boldsymbol{u}||^2 d\boldsymbol{x} \end{aligned} \tag{8}$$

The gradient of E w.r.t. $\boldsymbol{u}$ is $\frac{\partial E}{\partial \boldsymbol{u}} = \nabla_{\boldsymbol{u}} F_{in}(\boldsymbol{u}) + \nabla_{\boldsymbol{u}} F_{out}(\boldsymbol{u}) + \beta \Delta \boldsymbol{u}$, where $\nabla_{\boldsymbol{u}}$ denotes the functional gradient w.r.t. $\boldsymbol{u}$. We obtain the PDE (over domain Ω) whose steady state solution gives the minimizer displacement field $\boldsymbol{u}$ which varies over space :

$$\begin{aligned} \frac{\partial \boldsymbol{u}(\boldsymbol{x}, t)}{\partial t} &= \nabla_{\boldsymbol{u}} \hat{f}_{in}(\boldsymbol{x} + \boldsymbol{u}(\boldsymbol{x}))\ H(\hat{\Phi}(\boldsymbol{x} + \boldsymbol{u}(\boldsymbol{x}))) \\ &+ \nabla_{\boldsymbol{u}} \hat{f}_{out}(\boldsymbol{x} + \boldsymbol{u}(\boldsymbol{x}))\ (1 - H(\hat{\Phi}(\boldsymbol{x} + \boldsymbol{u}(\boldsymbol{x})))) \\ &+ \hat{f}(\boldsymbol{x} + \boldsymbol{u}(\boldsymbol{x}))\ \delta(\hat{\Phi}(\boldsymbol{x} + \boldsymbol{u}(\boldsymbol{x}))) \nabla \hat{\Phi}(\boldsymbol{x} + \boldsymbol{u}(\boldsymbol{x})) \\ &+ \beta \Delta \boldsymbol{u}(\boldsymbol{x}) \\ \boldsymbol{u}(\boldsymbol{x}, 0) &= \boldsymbol{u}_o(\boldsymbol{x}) \end{aligned} \tag{9}$$

Due to a narrowband level set implementation, we will most effectively be solving for $\boldsymbol{u}(\boldsymbol{x})$ on a band around the surface.

If we choose as a special case, a piecewise (p-w) constant model [13] (popularly known as "Chan-Vese" type flows) for the target regions that are to be segmented and registered in images I and $\hat{I}$, the region-based term in the energy, and the gradient terms are given by:

$$\begin{aligned} \hat{f} = \hat{f}_{in} - \hat{f}_{out} &= 2(\hat{m}_{in} - \hat{m}_{out})(\frac{\hat{m}_{in} + \hat{m}_{out}}{2} - \hat{I}(\boldsymbol{x} + \boldsymbol{u}(\boldsymbol{x}))), \\ \nabla_{\boldsymbol{u}} \hat{f}_{in} &= 2(\hat{I}(\boldsymbol{x} + \boldsymbol{u}(\boldsymbol{x})) - \hat{m}_{in}) \nabla \hat{I}(\boldsymbol{x} + \boldsymbol{u}(\boldsymbol{x})) \\ \nabla_{\boldsymbol{u}} \hat{f}_{out} &= 2(\hat{I}(\boldsymbol{x} + \boldsymbol{u}(\boldsymbol{x})) - \hat{m}_{out}) \nabla \hat{I}(\boldsymbol{x} + \boldsymbol{u}(\boldsymbol{x})), \end{aligned}$$

where $\hat{m}_{in}$ and $\hat{m}_{out}$ are the mean of the image intensities inside and outside the surface mapped onto the second image volume domain respectively. These expressions can be inserted into (9) to obtain the PDE, which flows in the gradient descent direction, for evolution of non-rigid registration field for the p-w constant region model:

$$\begin{aligned} \frac{\partial \boldsymbol{u}(\boldsymbol{x}, t)}{\partial t} &= -(\hat{m}_{in} - \hat{m}_{out})[\frac{(\hat{m}_{in} + \hat{m}_{out})}{2} - \hat{I}(\boldsymbol{x} + \boldsymbol{u}(\boldsymbol{x}))] \\ &\quad \delta(\hat{\Phi}(\boldsymbol{x} + \boldsymbol{u}(\boldsymbol{x}))) \nabla \hat{\Phi}(\boldsymbol{x} + \boldsymbol{u}(\boldsymbol{x})) \\ &- (\hat{I}(\boldsymbol{x} + \boldsymbol{u}(\boldsymbol{x})) - \hat{m}_{in}) \nabla \hat{I}(\boldsymbol{x} + \boldsymbol{u}(\boldsymbol{x}))\ H(\hat{\Phi}(x + \boldsymbol{u}(\boldsymbol{x}))) \\ &- (\hat{I}(\boldsymbol{x} + \boldsymbol{u}(\boldsymbol{x})) - \hat{m}_{out}) \nabla \hat{I}(\boldsymbol{x} + \boldsymbol{u}(\boldsymbol{x})) \cdot \\ &\qquad (1 - H(\hat{\Phi}(\boldsymbol{x} + \boldsymbol{u}(\boldsymbol{x})))) \\ &+ \frac{\beta}{2} \Delta \boldsymbol{u}(\boldsymbol{x}) \\ \boldsymbol{u}(\boldsymbol{x}, 0) &= \boldsymbol{u}_o(\boldsymbol{x}) = \boldsymbol{0}, \end{aligned} \tag{10}$$

where a zero vector field initialization is adequate in solving the PDE without any prior knowledge of the true vector field $\boldsymbol{u}$.

In some segmentation applications, the basic approach of thresholding has proven to be useful. Instead of using means inside and outside the surface, one can convert such a basic "Chan-Vese" flow to a "thresholding" flow. This is also equivalent to region growing to separate the intensity inside the growing surface from the outside by the given threshold. For this purpose we use the following speed function:

$$\hat{f} = (\hat{m}_{in} - \hat{m}_{out})(T - \hat{I}(\boldsymbol{x} + \boldsymbol{u}(\boldsymbol{x}))) \tag{11}$$

where the $\frac{\hat{m}_{in} + \hat{m}_{out}}{2}$ quantity in "Chan-Vese" flow is replaced by an arbitrary threshold T. For this speed function we use the following PDE for updating the vector field:

$$\begin{aligned} \frac{\partial \boldsymbol{u}(\boldsymbol{x}, t)}{\partial t} &= -(\hat{m}_{in} - \hat{m}_{out})(T - \hat{I}(\boldsymbol{x} + \boldsymbol{u}(\boldsymbol{x}))) \\ &\quad \delta(\hat{\Phi}(\boldsymbol{x} + \boldsymbol{u}(\boldsymbol{x}))) \nabla \hat{\Phi}(\boldsymbol{x} + \boldsymbol{u}(\boldsymbol{x})) + \frac{\beta}{2} \Delta \boldsymbol{u}(\boldsymbol{x}) \\ \boldsymbol{u}(\boldsymbol{x}, 0) &= \boldsymbol{u}_o(\boldsymbol{x}) = \boldsymbol{0}, \end{aligned} \tag{12}$$

applied to the boundary term only.

One can note that although the flows are presented for between two image domains, this idea can be extended to multiple coordinate spaces to non-rigidly register a single common contour with multiple target objects.

4. Results

Validation Studies: The synthetic green image volume in Fig.1 is deformed with a known 3D diverging vector field $\boldsymbol{v} = 10\,(x, y, z)^T$ to produce a second synthetic image volume. Then the vector field $\boldsymbol{u}$ between these two volumes is estimated using the flow in Eq.(10), with a zero vector field initial condition, on the first volume, in Fig. 5. The resulting estimated vector field is diverging as depicted inside on the first volume towards the inflated volume outside, and has a uniform magnitude (blue color of vector field magnitude is mapped to one and red is mapped to zero). The

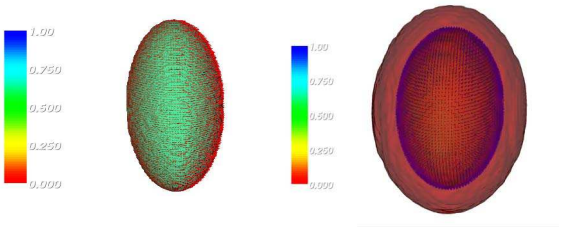

Figure 5. Starting with a surface on the green volume and a zero vector field, the surface deforms towards the red volume (on the right) shown along with the correct diverging vector field.

Distortion Measure	Error
Average Angle($\boldsymbol{u}_{GT} - \boldsymbol{u}_{EST}$)	0.07 π (13^o)
Standard Deviation Angle($\boldsymbol{u}_{GT} - \boldsymbol{u}_{EST}$)	0.04 π (7^o)
MSE ($\boldsymbol{u}_{GT} - \boldsymbol{u}_{EST}$)	1.65

Table 1. The average and standard deviation of the angle between GT and the estimated vector field, and the mean-squared error.

average error between the ground truth $\boldsymbol{v}$ and the estimated $\boldsymbol{u}$, $\frac{\int_{\boldsymbol{S}} ||\boldsymbol{u}-\boldsymbol{v}||_\infty dA}{\int_{\boldsymbol{S}} dA}$ turned out to be 0.62.

We simulated a non-rigid deformation on real input data, in Fig. 6, showing an image segment with a lymph node in an MR image sequence. The comparison is done using the angle between the ground truth deformation field and the estimated deformation field obtained with Eq. 10. The results displayed in the Table. 1 show an average angle difference of 13^o with a standard deviation of 7^o. The mean squared error between these two vector fields is found to be 1.65. Note that using a rigid transformation to match these two target regions results in a failure as depicted in Fig. 7.

The computational complexity of the algorithm is as follows. Since we are computing the PDEs in Eqs. (7) and (10) over a narrow-band around the zero level set of the surface in $\mathbb{R}^3$ (usually radius of the band is chosen as 5), the general complexity is $O(N^2)$. For the computation of the means inside and outside the image volume for Eq. (7), the complexity is $O(N^2)$ except at initialization it is $O(N^3)$ (going through all the image volume). For the computation of the means inside and outside the second image volume for Eq. (10) or (12), the second band (surface) is initialized after the first band (surface) is updated every time, therefore with the current implementation the complexity is $O(N^3)$, but it is possible to compute it at $O(N^2)$.

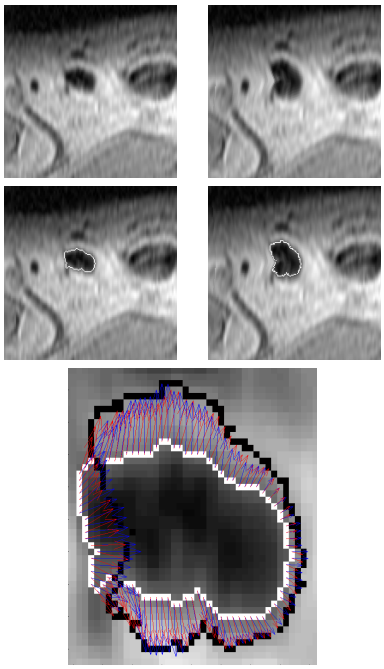

Figure 6. Left: MR image segment including a lymph node without (top) and with the converged contour (middle) ; Right : Deformed image with a known vector field without (top) and with the converged contour (middle). Bottom : Zoomed section showing the ground truth (GT) vector field (blue) and the estimated vector field (red).

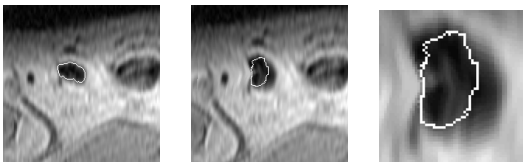

Figure 7. Using the rigid transformation flow in Eq. 3 results in a failure of the contour on the second image to match target region.

When the target structures in the two image domains do not overlap, either automated pre-processing using Dicom header information for physical coordinates to initialize the vector field or first jointly executing a rigid registration flow are possible solutions.

In Figure 8, two different slices of an MR image sequence depict the bladder which appears as a dark structure in the middle, and which is jointly registered and segmented by the PDEs (10) and (7). The result of deforming the sec-

ond image region of interest (that is around and inside the contour) with the estimated vector field towards the first image particularly shows the success of the estimation.

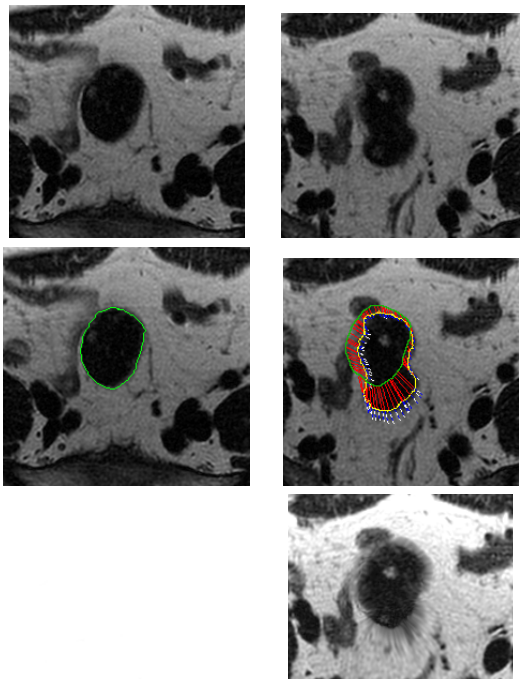

Figure 8. A 2D MR image pair at different slice levels (row 1). The bladder's deformation is recovered by the Eqns. (10),(7)) depicted with the vector field whose direction goes from red to blue(row 2), i.e., green contour to yellow contour. The second image is deformed by the estimated vector field (row 3).

Next we show an example for segmentation and registration of corpus callosum from MR brain image volumes. In neurology and neurocognitive science, the size and shape of the corpus callosum in human brain has shown to be correlated to different factors of humans and the human brain [10]. Therefore, inter-patient studies of corpus callosum(cc) characteristics is an important problem and requires estimation of transformations among cc shapes in a population of patients. We jointly segment and estimate a vector field between two different patients cc shapes as demonstrated in Figure 9 which shows evolution of the surface and the final estimated deformation field between the cc of the two patients. For inter-patient studies, such a vector field may be used to obtain a measure of shape and size differences between surfaces and thus proves to be useful.

Figure 10 shows the slices during the evolution. In this experiment, the "Chan-Vese" flow easily leaks to surrounding regions during the evolutions, therefore does not

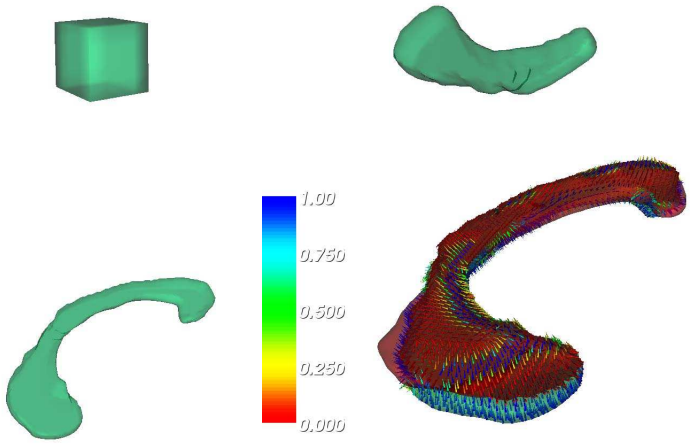

Figure 9. Evolution of the surface over the corpus callosum (top and bottom left) along with the estimated vector field from the first patient's corpus callosum (shown in green) towards the second one (shown in red).

perform successfully. Instead the "thresholding" flow in Eq. (12) along with the corresponding surface evolution flow Eq. (7) are used with a threshold of $T = 60$ whereas the image volumes has the intensity range (0,255). Therefore, with a simple modification to the simplest piecewise constant model and with a quickly obtained prior information from the intensity in the initialized seed surface, we could obtain a reasonable segmentation and registration result.

In the last example in Figure 11, two CT image volumes of the same patient taken at different time points are segmented and registered using Eqs. (7)-(10) for delineating the bladder volume at different time periods.

For a multi-modality application, for instance, a post-contrast T2-weighted MR image and a T2* echo weighted MR image, are shown in Fig. 12, where the regions and boundaries of a target structure, a malignant node, exhibit different characteristics. We utilize the piecewise constant model with a non-unit variance:

$$\begin{aligned}\frac{\partial \boldsymbol{u}(\boldsymbol{x},t)}{\partial t} = &-\frac{(\hat{I}(\boldsymbol{x}+\boldsymbol{u})-\hat{m}_{in})^2}{\hat{\sigma}_{in}^2}+\frac{(\hat{I}(\boldsymbol{x}+\boldsymbol{u})-\hat{m}_{out})^2}{\hat{\sigma}_{out}^2}\\ &\delta(\hat{\Phi}(\boldsymbol{x}+\boldsymbol{u}(\boldsymbol{x})))\nabla\hat{\Phi}(\boldsymbol{x}+\boldsymbol{u}(\boldsymbol{x}))\\ &-2\frac{(\hat{I}(\boldsymbol{x}+\boldsymbol{u}(\boldsymbol{x}))-\hat{m}_{in})}{\hat{\sigma}_{in}^2}\nabla\hat{I}(\boldsymbol{x}+\boldsymbol{u}(\boldsymbol{x}))\ H(\hat{\Phi}(x+\boldsymbol{u}(\boldsymbol{x})))\\ &-2\frac{(\hat{I}(\boldsymbol{x}+\boldsymbol{u}(\boldsymbol{x}))-\hat{m}_{out})}{\hat{\sigma}_{out}^2}\nabla\hat{I}(\boldsymbol{x}+\boldsymbol{u}(\boldsymbol{x}))\cdot\\ &\qquad(1-H(\hat{\Phi}(\boldsymbol{x}+\boldsymbol{u}(\boldsymbol{x}))))\\ &+\beta\Delta\boldsymbol{u}(\boldsymbol{x})\end{aligned} \tag{13}$$

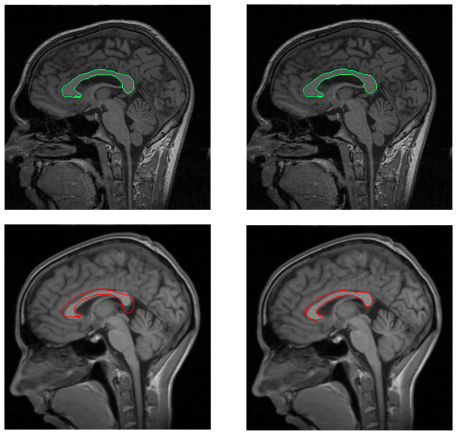

Figure 10. MR image slices from two different patients showing the mis-registration between the corpus callosum are given on the left; after the non-rigid registration and segmentation has been applied the result is shown on the right.

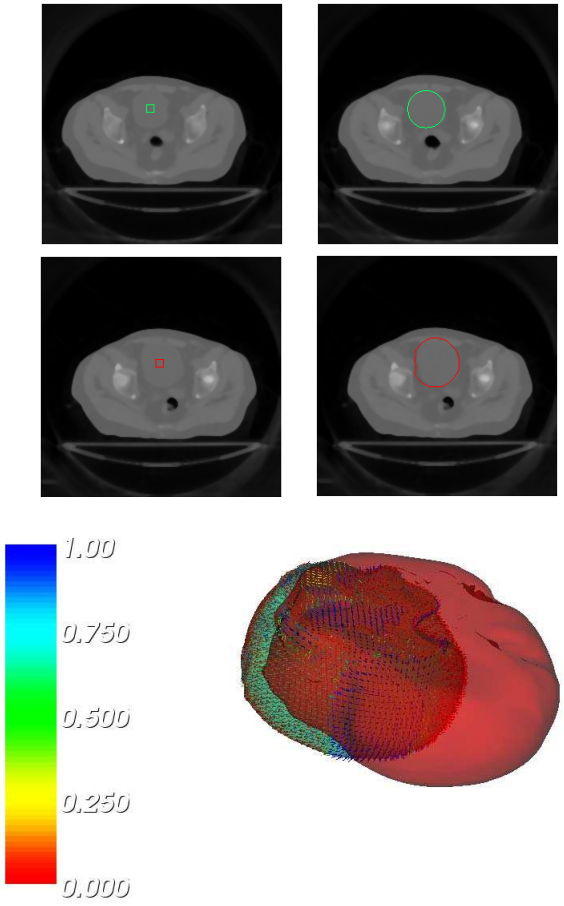

Figure 11. CT image slices of a patient at different times. A seed is given in the bladder (on the left) and the resulting segmentation and registration on the bladder (on the right). The surface shows the deformation of the first surface towards the second.

to obtain the deformation field between the nodes in T2 and T2* echo images. However, in multi-modality applications like this one, it is expected that utilizing more features to explain and account for a variety of region and boundary characteristics is desirable. One future extension of our work includes incorporation of boundary-based information in deriving the non-rigid registration PDE or using piecewise-smooth region models.

5. Conclusions

The contribution of this paper is an algorithm for joint segmentation and registration in infinite dimensions through coupling of two PDEs for surface and deformation field evolutions. Note that the desired coupling comes from estimating the common surface and its non-rigid deformations onto a target image. The solutions of these two PDEs both decrease the total energy of the surface, therefore aid each other in finding a locally optimal solution to the problem. The success of the algorithm in its current form depends on how well the region descriptor f represents the regions in the images, however, it can utilize more complicated statistical descriptors and information-theoretic measures, a direction to be explored. For target regions with large image clutter, inclusion of shape priors may be necessary. In that case, one can incorporate into this framework as well a mean shape from a training phase to penalize the surface deviations from the desired shape model. However, the framework we propose is general in the sense that inclusion of shape priors is not required, and the algorithm can proceed without any training phase but in the existence of a seed put somewhere around the target region of interest.

A more in depth validation for the presented algorithm is required but our studies have shown that the joint non-rigid registration and segmentation nicely generalizes the previous rigid framework, and is promising in its application to detection and analysis of non-rigid structures in multiple number of image volumes.

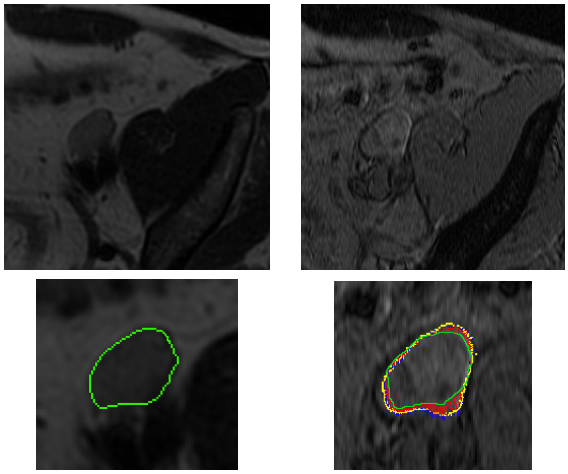

Figure 12. Using the non-unit variance flow (13), the node on the T2 image (green) is morphed onto the node on the T2* echo image (yellow) on the right.

6. Acknowledgements

We thank Jason Tyan and Tong Fang at Siemens Corporate Research, Princeton NJ, for supporting this work.

References

[1] L. Alvarez, J. Weickert, and J. Sánchez. Reliable estimation of dense optical flow fields with large displacements. *International Journal of Computer Vision*, 39(1):41–56, 2000.

[2] Y. Amit. A nonlinear variational problem for image matching. *SIAM Journal on Scientific Computing*, 15(1):207–224, 1994.

[3] G. Aubert, R. Deriche, and P. Konrprobst. Computing optical flow via variational techniques. *SIAM Journal of Applied Mathematics*, 60(1):156–182, 1999.

[4] M. Audette, F. Ferrie, and T. Peters. An algorithmic overview of surface registration techniques for medical imaging. *MIA*, 4(3):201–217, 2000.

[5] T. Chan and L. Vese. An active contour model without edges. In *Int. Conf. Scale-Space Theories in Computer Vision*, pages 141–151, 1999.

[6] C. Chefd'hotel, G. Hermosillo, and O. Faugeras. A variational approach to multi-modal image matching. In *VLSM Workshop-ICCV*, pages 21–28, 2001.

[7] Y. Chen, H. Tagare, S. Thiruvenkadam, F. Huang, D. Wilson, K. Gopinath, R. Briggs, and E. Geiser. Using prior shapes in geometric active contours in a variational framework. *Int. J. Computer Vision*, 50(3):315–328, 2002.

[8] D. Cremers and S. Soatto. Variational space-time motion segmentation. In *Proc. Int. Conf. on Computer Vision*, pages 886–982, 2003.

[9] I. Dydenko, D. Friboulet, and I. Magnin. A variational framework for affine registration and segmentation with shape prior: application in echocardiographic imaging. In *VLSM Workshop-ICCV*, pages 201–208, 2003.

[10] A. Lundervold, T. Taxt, N. Duta, and A. Jain. Model-guided segmentation of corpus callosum in mr images. In *Proc. IEEE Conf. on Computer Vision and Pattern Recognition*, pages 1231–1236, 1999.

[11] J. Maintz and M. Viergever. A survey for medical image registration. *Medical Image Analysis*, 2(1):1–36, 1998.

[12] T. McInerney and D. Terzopoulos. Deformable models in medical image analysis: A survey. *Medical Image Analysis*, 1(2):91–108, 1996.

[13] D. Mumford and J. Shah. Boundary detection by minimizing functionals. In *Proc. IEEE Conf. on Computer Vision and Pattern Recognition*, pages 22–26, San Fransisco, 1985.

[14] S. Osher and J. Sethian. Fronts propagating with curvature dependent speed: Algorithms based on the Hamilton-Jacobi formulation. *J. Computational Physics*, 49:12–49, 1988.

[15] N. Paragios and R. Deriche. Geodesic active regions for motion estimation and tracking. In *Proc. Int. Conf. on Computer Vision*, pages 224–240, 1999.

[16] N. Paragios, M. Rousson, and M. Ramesh. Knowledge-based registration and segmentation of the left ventricle: A level set approach. In *IEEE Workshop on App. Comp. Vision*, pages 37–42, 2002.

[17] J. Pluim, J. Maintz, and M. Viergever. Mutual-information-based registration of medical images: A survey. *IEEE Trans. Medical Imaging*, 22:986–1004, 2003.

[18] F. Richard and L. Cohen. A new image registration technique with free boundary constraints: Application to mammography. In *Proc. European Conf. Computer Vision*, pages 531–545, 2002.

[19] B. Vemuri and Y. Chen. *Geometric Level Set Methods in Imaging, Vision and Graphics, Eds. S.Osher and N.Paragios*, chapter Joint Image Registration and Segmentation, pages 251–269. Springer Verlag, 2003.

[20] P. Wyatt and J. Noble. Map mrf joint segmentation & registration. In *MICCAI*, pages 580–587, 2002.

[21] A. Yezzi, L. Zollei, and T. Kapur. A variational framework for joint segmentation and registration. In *CVPR-MMBIA*, pages 44–49, 2001.

[22] A. Yezzi, L. Zollei, and T. Kapur. A variational framework for integrating segmentation and registration through active contours. *Medical Image Analysis*, 7(2):171–185, 2003.

[23] T. Zhang and D. Freedman. Tracking objects using density matching and shape priors. In *Proc. Int. Conf. on Computer Vision*, pages 1056–1062, 2003.